Journal of Materials Chemistry C

PAPER

View Article Online
View Journal

Cite this: DOI: 10.1039/c8tc02153h

Ultra-stable 2D layered methylammonium cadmium trihalide perovskite photoelectrodes†

Hsien-Yi Hsu, ‡*[abc] Li Ji,‡*[a] Chengxi Zhang,[bc] Chun Hong Mak,[bc] Rugeng Liu,[bc] Tie Wang,[d] Xingli Zou,[e] Shao-Yuan Leu[f] and Edward T. Yu[a]

Received 3rd May 2018,
Accepted 17th September 2018

DOI: 10.1039/c8tc02153h

rsc.li/materials-c

For the first of time, we demonstrate that methylammonium cadmium halides show photoelectrochemical (PEC) response with excellent humidity and chemical resistance because the oxidation state of almost all cadmium compounds is +2. The photocurrent densities of two-dimensional (2D) layered $(MA)_2CdCl_4$ perovskites are about 0.30 mA cm^{-2} under 100 mW cm^{-2} irradiation. The interaction between these methylammonium cadmium halides and water vapor is studied by probing film morphology and characterizing single crystal structure. It is shown that H_2O is able to complex with the perovskite, forming a hydrate product with the molecular formula of $MACd_3Cl_7{\cdot}3H_2O$ upon humidity exposure. This causes a decrease in absorption and a recognizable change in the crystal structure of the material. When compared to methyl-ammonium lead iodide ($MAPbI_3$), the PEC stability of 2D layered $(MA)_2CdCl_4$ perovskites with $BQ/BQ^{\bullet-}$ redox couples (where BQ is benzoquinone) in CH_2Cl_2 is enhanced from 50 hours to 600 hours, exhibiting an increase of 12 times.

Introduction

Hybrid organic–inorganic halide perovskites have been extensively studied due to their remarkable optical and electronic features such as high absorption coefficient, long exciton diffusion length, excellent carrier transport and low exciton binding energy, as well as a facile solution process for the fabrication of organic–inorganic halide perovskites.[1–8] Tin-based hybrid perovskites, such as methylammonium tin triiodide ($MASnI_3$) and formamidinium tin triiodide ($FASnI_3$), have been investigated as both absorbers[9,10] and emitters[11,12] in optoelectronic devices with promising performances. However, the rapid oxidation of Sn^{2+} to Sn^{4+} (even in a nitrogen atmosphere) and uncontrollable crystal growth lead to extremely poor stability and reproducibility of Sn-based perovskites. Much effort has been directed toward these practical barriers for commercial applications of different hybrid perovskites.[13,14] Beyond Sn-based hybrid perovskites, hybrid organic–inorganic perovskites with the general formula ABX_3 or A_2BX_4 exhibit a wide range of fascinating properties.[13,14] One of the important aspects that makes hybrid perovskites successful is the adaptability of this structure type towards A, B or X site substitution, which allows for tailoring of properties to meet particular requirements.[15,16] A central principle in the development of hybrid organic–inorganic perovskites is Goldschmidt's Tolerance Factor (GTF),[17] which can evaluate ionic size mismatches which the perovskite-structure will tolerate until a different structure-type is formed, $\alpha = (r_A + r_X)/\sqrt{2}(r_B + r_X)$, where r_i is the radii of ions in the perovskite ABX_3, and i = A, B and X, respectively. Generally, it is possible that hybrid perovskites could be formed for TFs between 0.8 and 1.

To develop ultra-stable hybrid perovskite photoelectrodes, we initially identified a series of potential hybrid materials with perovskite-like structures by GTF, *i.e.*, $(MA)_2MnCl_4$, $(MA)_2GeCl_4$, $(MA)_2EuCl_4$, $(MA)_2CdCl_4$, $(MA)_2FeCl_4$ and $(MA)_2CuCl_4$. Building on our previous work with the array scanning technique for the analysis of $MAPbI_3$,[18] we undertook a detailed study on a variety of potential hybrid perovskites using the high-throughput scanning electrochemical microscopy (SECM) system (Fig. S1, ESI†). This combinatorial screening technique can reduce the effort and materials expended in the optimization process, and

[a] Microelectronics Research Center, Department of Electrical and Computer Engineering, University of Texas, Austin, Texas 78758, USA. E-mail: nmgjili@utexas.edu
[b] School of Energy and Environment & Department of Materials Science and Engineering, City University of Hong Kong, Kowloon Tong, Hong Kong, China. E-mail: sam.hyhsu@cityu.edu.hk
[c] Shenzhen Research Institute of City University of Hong Kong, Shenzhen 518057, P. R. China
[d] Beijing National Laboratory for Molecular Sciences, Key Laboratory of Analytical Chemistry for Living Biosystems, Institute of Chemistry, Chinese Academy of Sciences, Beijing 100190, P. R. China
[e] State Key Laboratory of Advanced Special Steel & School of Materials Science and Engineering, Shanghai University, Shanghai 200072, P. R. China
[f] Department of Civil & Environmental Engineering, The Hong Kong Polytechnic University, Hung Hom, Kowloon, Hong Kong SAR, P. R. China

† Electronic supplementary information (ESI) available. CCDC 1840952, 1840955 and 1837551. For ESI and crystallographic data in CIF or other electronic format see DOI: 10.1039/c8tc02153h

‡ Dr H.-Y. Hsu and Dr L. Ji contributed equally to this work.

evaluate the photocurrent response on the semiconductor array. The $(MA)_2CdCl_4$ perovskite alternative results in the highest photocurrent density in the quantitative SECM image. Up to now, studies related to methylammonium cadmium halides are extremely rare. The crystal structure has been characterized for compounds with the chemical composition $(MA)_2CdCl_4$, which is found to be isostructural at room temperature with $(MA)_2MnCl_4$ with the orthorhombic space group *Cmca*.[19] As far as we know, the photoelectrochemical (PEC) or photovoltaic property of Cd-based hybrid perovskite materials has never been investigated. Here, by utilizing the photoelectrochemical system we designed, we confirmed the photocurrent density of $(MA)_2CdCl_4$-based bulk film photoelectrodes, showing around 0.30 mA cm^{-2} under irradiation. Single crystals of $MACdI_3$ and $(MA)_2CdCl_4$ displaying 2D- and 3D-perovskite crystal structures were grown using stoichiometric precursors in a nitrogen atmosphere for the characterization of materials and structures. By using a UV-vis spectrometer, we found that the absorbance of these Cd-based hybrid perovskites in the ultraviolet region from 200 to 335 nm could seriously restrict the collection of photons, resulting in the poor photoelectrochemical responses.

The photoluminescence decay was also measured to explore the dynamics of exciton transfer. To assess the effect of humidity on light absorption and PEC performance in high humidity, UV-vis absorption and PEC stability were tested for Cd-based hybrid materials stored at 90% RH. After 60 days exposure, the formation of a crystal hydrate product on $(MA)_2CdCl_4$ perovskites causes ~60% decrease in absorption across the ultraviolet region of the spectrum. The 2D layered $(MA)_2CdCl_4$ perovskites stored at 90% RH underwent a decrease in PEC performance from initially 3.0 mA cm^{-2} to less than 1 mA cm^{-2} over 600 hours. By contrast, the absorption of $MAPbI_3$ thin films stored at 90% RH became very weak after 15 days. The PEC performance of $MAPbI_3$ films stored at 90% RH declined by more than 70% within only 50 hours. Therefore, in this work we demonstrate that the moisture stability of 2D layered Cd-based hybrid materials, $(MA)_2CdCl_4$, is increased by 12 times compared to that of $MAPbI_3$ (from 50 hours to 600 hours).

Results and discussion

A rapid screening method for semiconductor materials using a modified SECM imaging technology has been applied previously.[20] Briefly, arrays composed of ~350 μm diameter semiconductor spots with different compositions consisting of $(MA)_2MnCl_4$, $(MA)_2GeCl_4$, $(MA)_2EuCl_4$, $(MA)_2CdCl_4$, $(MA)_2FeCl_4$ and $(MA)_2CuCl_4$ were deposited by a piezoelectric dispenser onto a conductive fluorine-doped tin oxide (FTO) substrate. The scanning tip of the modified SECM was replaced by a 300 μm fiber optic connected to a xenon lamp and was rapidly scanned over the array. The SECM images using a rapid screening analysis on all potential hybrid perovskite alternatives were obtained (Fig. 1). The arrays contained three rows and six columns of spots. There are twelve spots of pure $(MA)_2MnCl_4$ perovskites in the top two rows to confirm the repeatable results in the SECM technique. The photocurrents of all 14 spots are almost the same (~0.65 ± 0.02 A). The third six-spot row we analyzed includes spot arrays of all potential hybrid

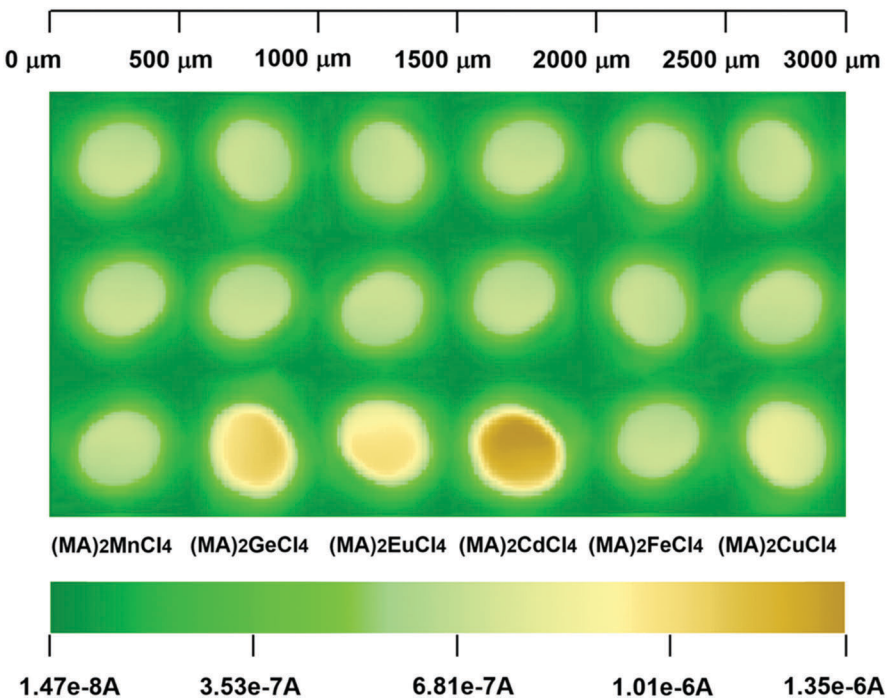

Fig. 1 SECM images demonstrating the typical photocurrent response of A_2BX_4 perovskites under irradiation. The color represents the measured photocurrent shown in the scale bar below the SECM image. The first and second six-spot rows are pure $(MA)_2MnCl_4$ perovskites. The third six-spot row includes $(MA)_2MnCl_4$, $(MA)_2GeCl_4$, $(MA)_2EuCl_4$, $(MA)_2CdCl_4$, $(MA)_2FeCl_4$ and $(MA)_2CuCl_4$ (from left to right) in each spot in the array electrode.

perovskites. The rapid screening results showed that $(MA)_2CdCl_4$ perovskites generated the highest photocurrent response under irradiation. We thus systematically investigated Cd-based hybrid perovskites utilizing morphology engineering, photophysical methods and photoelectrochemical techniques.

To explore the influence of chloride ions on Cd-based hybrid materials, we studied a series of hybrid Cd-based materials, referred to here as CD-1, CD-2, CD-3 and CD-4, prepared by solution-based processes from four different precursors including MAI, MACl, CdI_2 and $CdCl_2$. X-ray diffraction (XRD) was used to characterize the crystallinity of Cd-based hybrid materials. Because powders and single crystals could be found in CD-1, CD-2, CD-3 and CD-4 thin films, diffraction data were collected by using glancing incidence angle X-ray diffraction (XRD) with a CuKα radiation source and a Rigaku AFC12 diffractometer with the use of MoKα radiation (λ = 0.71073 Å), respectively (Fig. 2b). For CD-1 and CD-2, the single crystal diffraction data revealed the structure of $MACdI_3$ to be monoclinic (space group = $P21/n$), with unit cell parameters of a = 9.05(2) Å, b = 7.048(15) Å, c = 14.74(3) Å, α = 90.000, β = 90.230, and γ = 90.000 (Table S1, ESI†). According to crystal data and structure refinement of $MACdI_3$ in Table S1 (ESI†), each unit cell contains four molecules with the chemical formula of $MACdI_3$. The single crystals acquired in CD-3 and CD-4 thin films show the structure of $(MA)_2CdCl_4$ to be orthorhombic (space group = *Cmca*), with unit cell parameters of a = 7.391(2) Å, b = 19.636(6) Å, c = 7.5139(19) Å, α = 90.000, β = 90.000, and γ = 90.000 (Table S2, ESI†). Similarly, each unit cell containing one molecule with the chemical formula of $(MA)_2CdCl_4$ could be clarified by crystal data and structure refinement in Table S2 (ESI†).

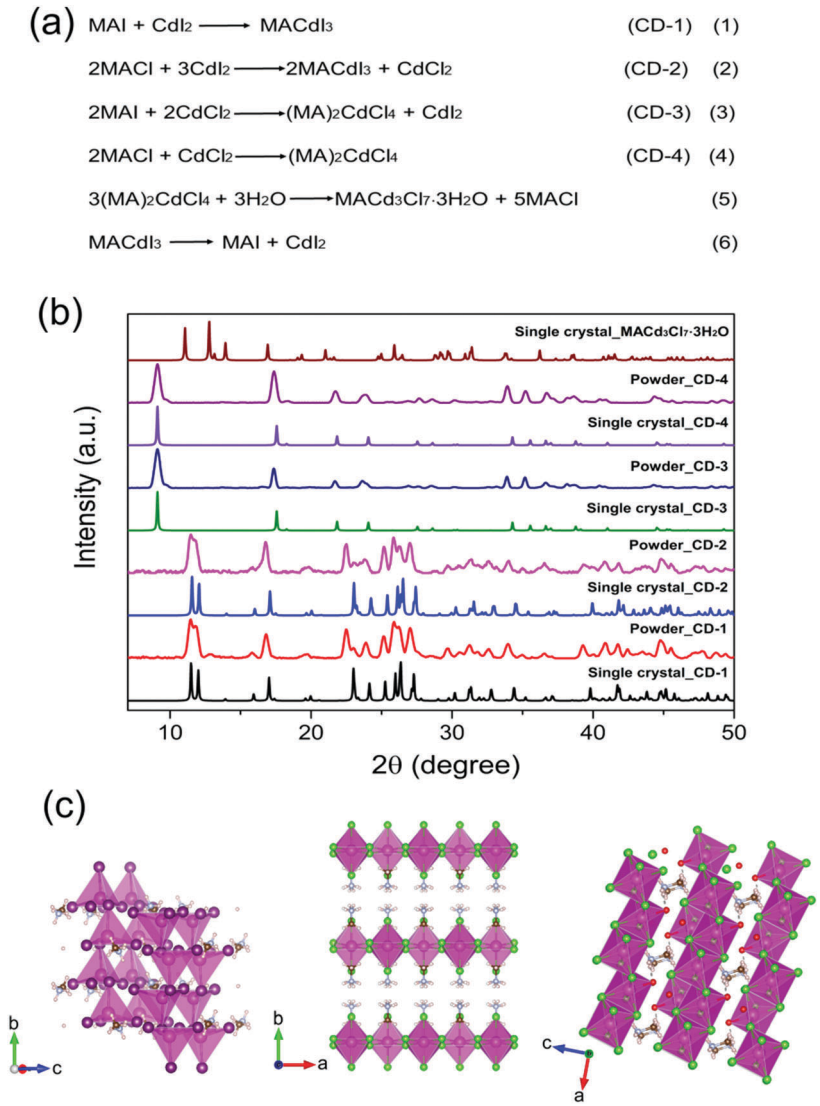

Fig. 2 (a) The formation and degradation processes of methylammonium cadmium halides (CD-1, CD-2, CD-3 and CD-4). (b) XRD patterns for single crystals of CD-1 (black), powders of CD-1 (red), single crystals of CD-2 (blue), powders of CD-2 (magenta), single crystals of CD-3 (green), powders of CD-3 (navy), single crystals of CD-4 (violet), powders of CD-4 (purple) and single crystals of $MACd_3Cl_7{\cdot}3H_2O$ (wine). (c) The crystal structures of $MACdI_3$, $(MA)_2CdCl_4$ and $MACd_3Cl_7{\cdot}3H_2O$. The colours represent the following: purple, Cd atom; dark purple, I atom; grey, C atom; dark brown, N atom; pink, H atom; green, Cl atom; red, O atom.

After exposure to 90% RH for 60 days, single crystal hydrate products were formed in CD-3 and CD-4 thin films. From single crystal diffraction data, the crystal structure of this hydrate, $MACd_3Cl_7{\cdot}3H_2O$, was determined to be monoclinic (space group = $P21/m$), with unit cell parameters of a = 6.7315(4) Å, b = 15.9916(9) Å, c = 6.9266(4) Å, α = 90.000, β = 90.922, and γ = 90.000 (Table S3, ESI†). The details of X-ray data collection and refinement parameters for $MACdI_3$, $(MA)_2CdCl_4$ and $MACd_3Cl_7{\cdot}3H_2O$ single crystals are given in the ESI.† Fig. 2b also shows the powder XRD patterns of CD-1, CD-2, CD-3 and CD-4 films. The diffraction peaks of the crystal powders are very similar to calculated patterns from single crystal diffraction data. The main peaks for CD-1 and CD-2 at 11.46°, 12.16°, 17.11°, 23.06°, 25.99°, 26.49°, and 27.30° are assigned to the (101), (002), (111), (202), (021), (212), and (014) planes, respectively. For CD-3 and CD-4, strong peaks at 9.14°, 17.51°, 21.75°, 34.06°, 35.27° and 36.28° are assigned to the (020), (111), (131), (202), (222) and (062) planes. The clear peaks of $MACd_3Cl_7{\cdot}3H_2O$ crystals at 11.16°, 12.97°, 13.98°, 17.01°, 21.14°, 25.99°, 31.44° and 36.28° are assigned to the (020), (001), (011), (021), (031), (140), (230) and (160) planes. As depicted in Fig. 2c, the inorganic anion in the crystal structure of $MACdI_3$ forms a CdI_4^{2-} tetrahedron. In contrast, the crystal structures of $(MA)_2CdCl_4$ and $MACd_3Cl_7{\cdot}3H_2O$ consist of assemblies of $CdCl_6^{4-}$ and $CdOCl_5^{5-}$ octahedra respectively. It is worth noting that $(MA)_2CdCl_4$ perovskite materials exhibit a 2D layered structure (Fig. 2c, middle) which matches with the previously reported XRD pattern.[19] Based on thin film and single-crystal XRD patterns in Fig. 2b, the possible chemical reactions for the formation of each Cd-based hybrid material, CD-1, CD-2, CD-3 and CD-4, are provided in Fig. 2a.

Scanning electron microscopy (SEM) characterization was performed to further investigate the surface morphology of CD-1, CD-2, CD-3 and CD-4 films. All films were prepared on FTO substrates to ensure identical conditions of the working device. Fig. 3a shows the top-view surface profile of CD-1 ($MACdI_3$) films deposited on the substrate, revealing rod-shaped structures with poor coverage. The coverage of CD-2 films is obviously increased by the formation of $CdCl_2$ (the 2nd chemical reaction of Fig. 2a), but some of the FTO substrate remains uncovered. In the morphology of CD-3 films (Fig. 3c), the $(MA)_2CdCl_4$ perovskites in the presence of CdI_2 species show small rice grains together with tiny rods. For CD-4, high surface coverage $(MA)_2CdCl_4$ perovskite films with high crystallinity, increased grain size and minimum pinholes were

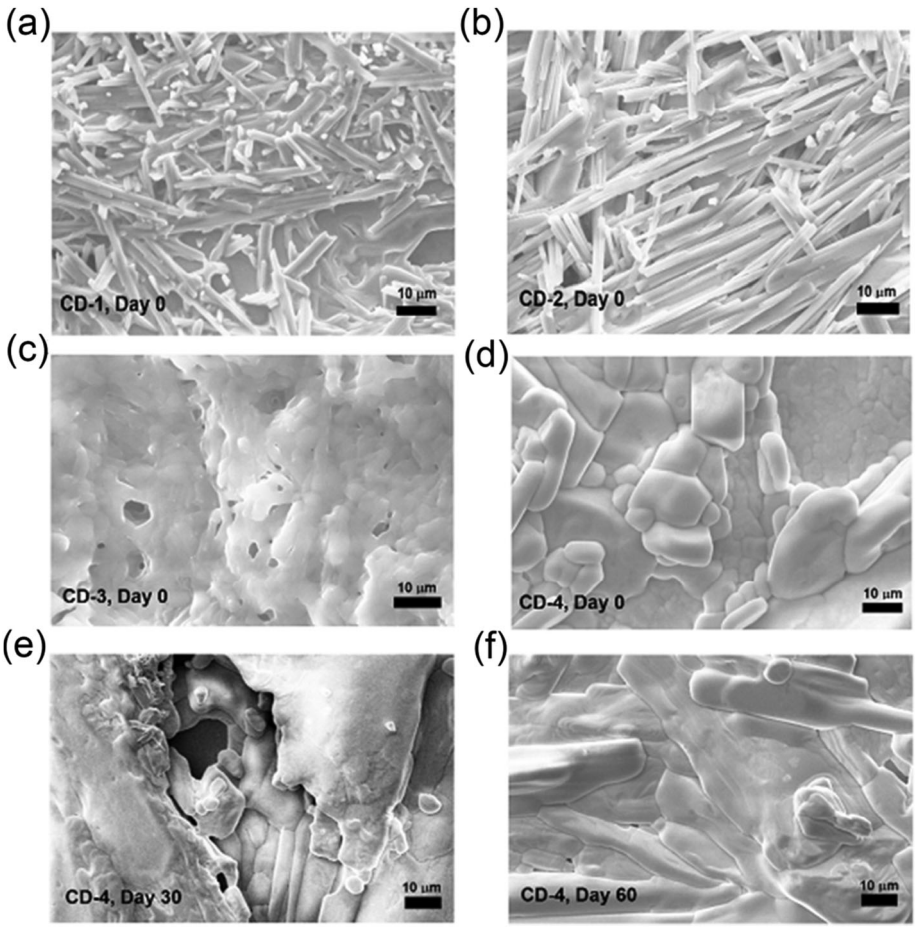

Fig. 3 (a) SEM image of CD-1 obtained immediately after film deposition. (b) SEM image of CD-2 obtained immediately after film deposition. (c) SEM image of CD-3 obtained immediately after film deposition. (d) SEM image of CD-4 obtained immediately after film deposition. (e) SEM image of CD-4 recorded after 30 days exposure to 90% RH. (f) SEM image of CD-4 recorded after 60 days exposure to 90% RH.

obtained (Fig. 3d). Fig. 3e and f shows SEM images of CD-4 films stored at 90% RH for 30 days and 60 days, respectively. The CD-4 film stored under 90% RH for 30 days exhibits a coarsening of the perovskite (Fig. 3e). However, the CD-4 perovskite becomes smooth and highly ordered by a recrystallization process after 60 days under 90% RH (Fig. 3f).

The absorption spectra of CD-1, CD-2, CD-3 and CD-4 films were measured at room temperature (Fig. 4a). The Cd-based hybrid materials show similar absorption spectra, which exhibit a single broad, featureless band with λ_{max} at 250 nm. In the inset of Fig. 4a, the absorbance in the 320–400 nm wavelength range for CD-3 and CD-4 is slightly higher than that for CD-1 and CD-2. According to the Kubelka–Munk equation,[21] the optical band gaps (E_g) of CD-1, CD-2, CD-3 and CD-4 were determined with a value of ~4.13 eV, which is close to the direct band gap calculated by density functional theory (Fig. S2, ESI†).

The steady-state photoluminescence (PL) spectra of CD-1, CD-2, CD-3 and CD-4 films were measured at room temperature under optical excitation with monochromatic laser light at 290 nm (Fig. 4b). Their PL spectra exhibit a strong band with the maximum at 440 nm and a weak shoulder at 385 nm which are assigned as fluorescence due to the short lifetime of this emission ($\tau < 1.5$ ns) (Fig. 4c).[18,22,23] PL decay dynamics can be applied to investigate exciton diffusion behaviors of Cd-based hybrid materials. Time-resolved PL spectra of CD-1, CD-2, CD-3 and CD-4 were then recorded using a time-correlated single photon counting (TCSPC) system to explore the PL decay dynamics. Excitation was provided by a 266 nm pulsed laser, which provided <200 ps pulses with a fluence of ~30 nJ cm^{-2}.[34] The PL decay at a wavelength of 440 nm was measured for CD-1, CD-2, CD-3 CD-4 and CD-4 (after exposure to 90% RH for 60 days) films deposited on FTO glass substrates, as shown in Fig. 4c and d. The PL lifetime, τ_{PL}, was determined by fitting exponential functions to the measured decay curves (Fig. 4c and d). The fitting parameters (τ_1, α_1, τ_2, α_2) and corresponding errors (R^2) of PL decay are summarized in Table S4 (ESI†). The CD-1 film exhibits a time constant of τ_{PL} = 0.20 ns owing to electronic defects at grain boundaries that lead to rapid recombination with low photocurrent density.[35] The lifetime in CD-2 films was increased to 0.40 ns, which was attributed to improved film quality arising from the formation of $CdCl_2$ (the 2nd chemical reaction of Fig. 2a), resulting in the reduction of free carrier recombination. As compared with CD-1 and CD-2, the fast decay component of CD-3 perovskites shows a time constant of τ_1 = 0.37 ns, likely due to bimolecular recombination;[24–26] the long decay component τ_2 is assigned to recombination of free

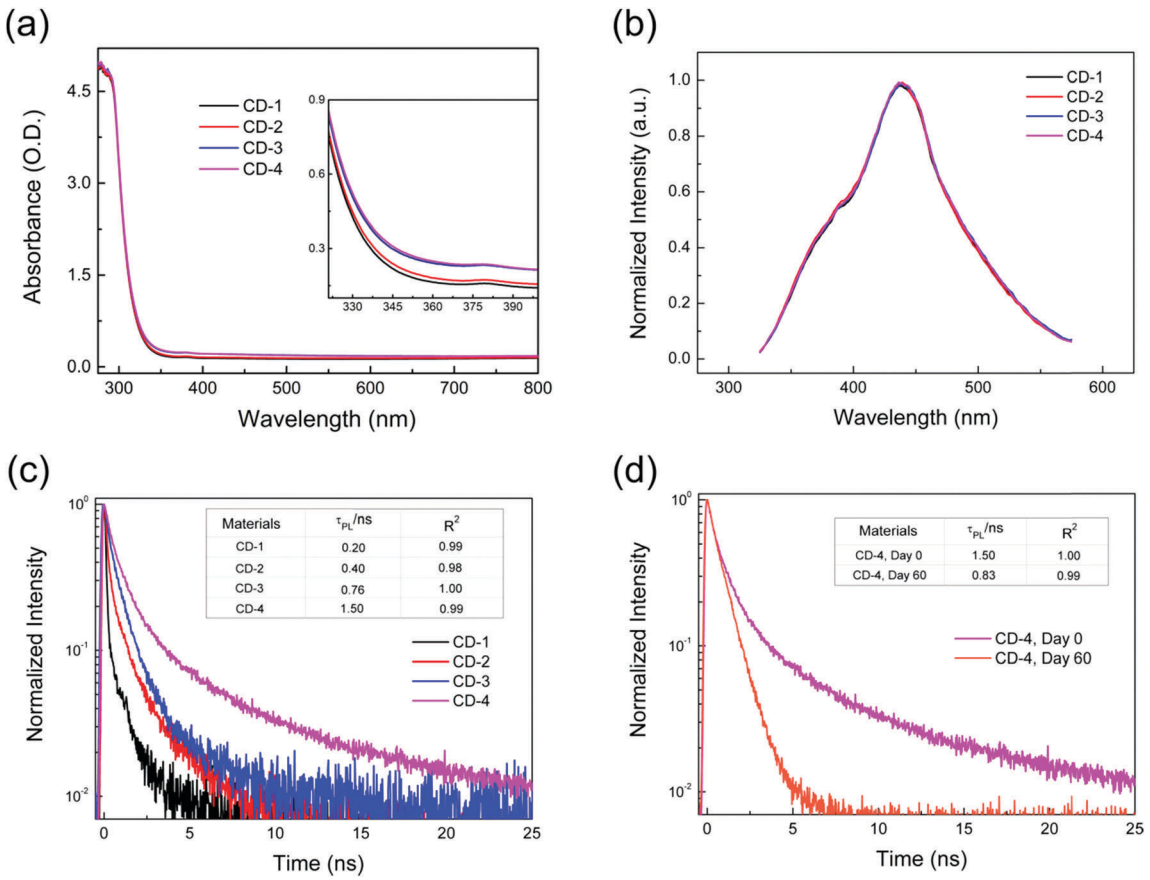

Fig. 4 (a) UV-vis absorption spectra of CD-1 (black), CD-2 (red), CD-3 (blue) and CD-4 (magenta). Inset, absorbance zoomed in the 320–400 nm wavelength range. (b) PL spectra of CD-1 (black), CD-2 (red), CD-3 (blue) and CD-4 (magenta). (c) PL decay monitored at 440 nm for CD-1 (black), CD-2 (red), CD-3 (blue) and CD-4 (magenta). (d) PL decay monitored at 440 nm for CD-4 (magenta) prepared immediately after film deposition and CD-4 (orange) stored after 60 days exposure to 90% RH.

carriers in the radiative channel.[27,28] For CD-4, the 2D layered $(MA)_2CdCl_4$ perovskite crystals give rise to a longer exciton diffusion lifetime with a time constant of τ_{PL} = 1.50 ns. After 60 days exposure to 90% RH, the lifetime of CD-4 films was reduced to 0.83 ns, because the emission intensity was quenched by the formation of hydrate products.

Fig. 5a shows the scheme of a PEC cell, which consists of one working electrode (Cd-based hybrid material film on an FTO substrate) for the production and detection of reduced species, and a platinum (Pt) mesh counter electrode to generate an oxidized mediator species O_x at a diffusion-limited rate from a reduced species (R_{ed}), which is formed by the working electrode in the electrolyte. The PEC responses of CD-1, CD-2, CD-3 and CD-4 for BQ reduction were characterized by linear sweep voltammetry (LSV) with chopped light under irradiation. Fig. 5b shows the LSV measurements for CD-1, CD-2, CD-3 and CD-4 films which were conducted from +0.40 to −0.70 V *vs.* Fc/Fc^+ at a scan rate of 50 mV s^{-1}. These Cd-based hybrid materials were photoactive in the reduction of BQ and exhibited a well-defined p-type behavior. The hybrid material $MACdI_3$ (CD-1) resulted in a very small cathodic photocurrent of ∼0.01 mA cm^{-2} at −0.7 V *vs.* Fc/Fc^+ with the onset at ∼0.35 V, which should be close to the valence band edge or flat band potential (E_{fb}). The CD-2 samples generated a photocurrent of 0.15 mA cm^{-2} with very similar onset potential for BQ reduction. While the CD-3 film shows a higher cathodic current flow (∼0.17 mA cm^{-2} at −0.7 V *vs.* Fc/Fc^+) with the onset potential at ∼0.30 V, the photocurrent for 2D layered $(MA)_2CdCl_4$ perovskites (CD-4) increases up to ∼0.30 mA cm^{-2} which is due to the improved perovskite crystallinity and grain size.

The absorption of the film at 275 nm for CD-1, CD-2, CD-3 and CD-4 stored at 0%, 50%, and 90% RH at room temperature was tracked in order to assess the degradation of Cd-based hybrid material films stored in different humidity environments (Fig. 5c). For comparison, absorption at 600 nm of $MAPbI_3$ films was also measured under the same conditions. As shown in Fig. 5c, CD-3 and CD-4 films stored at 90% RH still retained 35% of the initial absorption after 60 days of exposure. In the case of CD-1 and CD-2 films stored at 90% RH, the absorbance decreased by 80% in only 30 days. For $MAPbI_3$ films exposed to 90% RH, we could only detect very weak absorption at 600 nm after 15 days.

To explore the effect of humidity on PEC performance, liquid junction PEC cells, WE/CH_2Cl_2, $TBAPF_6$ (0.1 M), BQ (2 mM), $BQ^{\bullet-}$

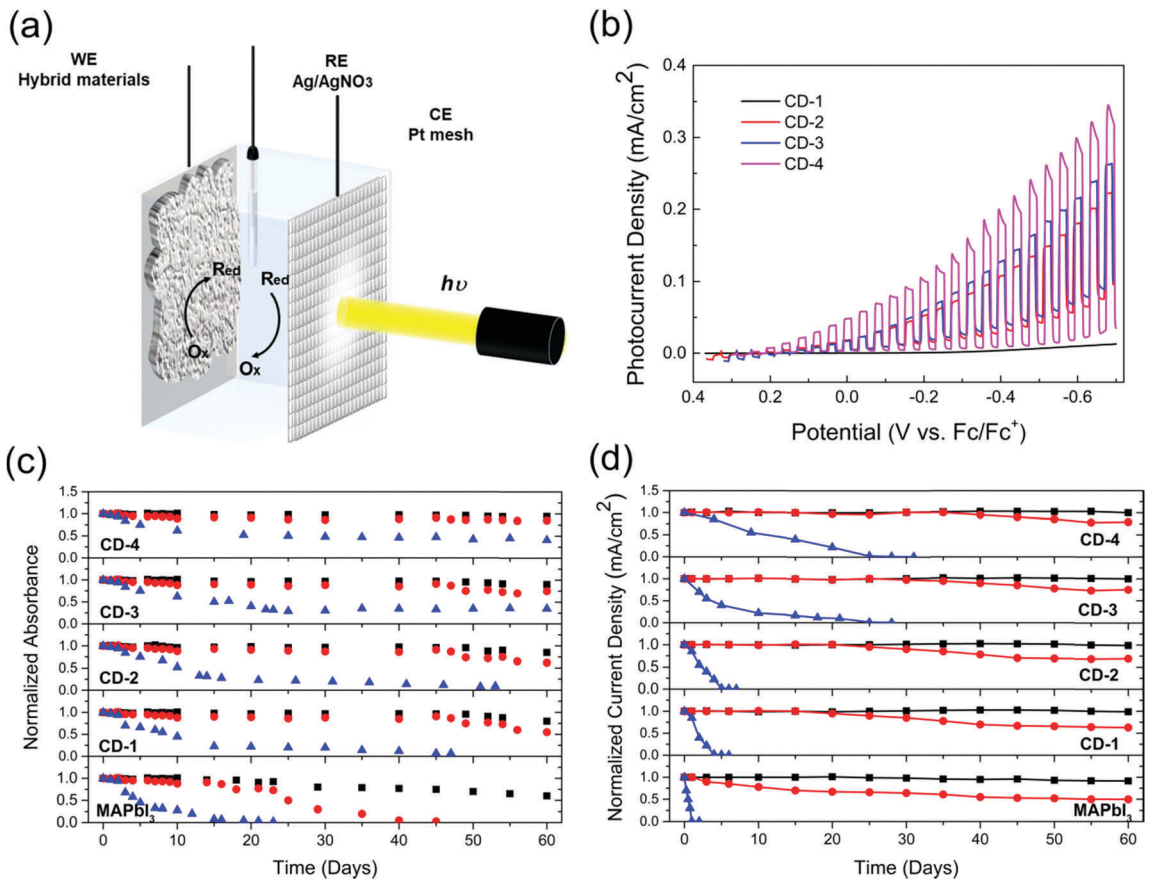

Fig. 5 (a) Schematic illustration of the photoelectrochemical test in a PEC cell using a standard three-electrode system. WE, CD-1, CD-2, CD-3, CD-4 or $MAPbI_3$; RE, $Ag/AgNO_3$; CE, Pt mesh. (b) LSV characteristics of CD-1 (black), CD-2 (red), CD-3 (blue) and CD-4 (magenta) under chopped illumination. (c) Absorption at 275 nm of CD-1, CD-2, CD-3 and CD-4 films stored at room temperature under 0% (■), 50% (●), and 90% (▲) RH. For comparison, absorption at 600 nm of $MAPbI_3$ films was measured under the same condition. (d) Photocurrent density of CD-1, CD-2, CD-3, CD-4 and $MAPbI_3$ films stored at 0% (■), 50% (●), and 90% (▲) RH.

(2 mM)/CE (WE: CD-1, CD-2, CD-3, CD-4 or $MAPbI_3$; CE: Pt mesh), were prepared. The photocurrent density as a function of time was investigated in PEC cells for Cd-based hybrid materials in different controlled humidity environments (*i.e.*, 0%, 50%, and 90% RH) under irradiation with a 100 mW cm^{-2} xenon lamp focused onto the photoelectrode (Fig. 5a). The PEC response obtained from photocurrent measurements was normalized to the initial value and the normalized values were plotted over the period of the experiment (Fig. 5d). The degradation of PEC performance was much slower for the films stored under 0% RH and 50% RH. The $MAPbI_3$-based PEC cells stored at 90% RH degraded completely within only 3 days. The photocurrent of CD-1 and CD-2 films under 90% RH underwent complete degradation after 7 days of exposure. The CD-3 film stored at 90% RH encountered a decline in PEC performance from initially 0.17 mA cm^{-2} to less than 0.01 mA cm^{-2} after 25 days. In the case of the CD-4 film stored at 90% RH, a reduction in PEC performance of ~99% took place over the 28 day experiment. Table S5 (ESI†) shows a comparison of the long-term stability of several perovskite materials under different testing conditions, including light/dark, temperature, humidity, and sealed/unsealed. Compared with previously reported perovskite materials, the 2D layered $(MA)_2CdCl_4$ perovskites in this work exhibit significantly enhanced stability, verifying the high quality of the $(MA)_2CdCl_4$ film, and consistent with the longer exciton diffusion lifetime discussed above.

Conclusions

In summary, we demonstrate for the first time that methylammonium cadmium halides exhibit PEC response and enhanced moisture stability. The photocurrent density of 2D layered $(MA)_2CdCl_4$ perovskites is ~0.30 mA cm^{-2} at −0.7 V *vs.* Fc/Fc^+ under 100 mW cm^{-2} irradiation. Degradation upon exposure to moisture appears to occur *via* the formation of a $(MA)_2CdCl_4$ hydrate, $MACd_3Cl_7{\cdot}3H_2O$, as determined from characterization of the single crystal structure of the degraded perovskite materials. The decomposition of hybrid materials or incorporation of H_2O leads to a loss in absorbance across the UV-vis spectrum. The performance of PEC cells was found to decrease much more rapidly than the UV-visible absorption of the methylammonium cadmium halide films. The PEC stability of $(MA)_2CdCl_4$ perovskites with $BQ/BQ^{\bullet -}$ redox couples is extended from 50 hours to 600 hours due to the stable +2 oxidation state of cadmium. This work demonstrates that 2D layered $(MA)_2CdCl_4$ perovskites could be a promising candidate for highly efficient and long-term stable optoelectronic devices, including but not limited to photodetectors, image sensors and light emitting diodes operating at UV wavelength.

Experimental

Material synthesis

Methylamine iodide (MAI) was prepared by reacting methylamine (33 wt% in ethanol; Sigma-Aldrich) with hydroiodic acid (HI) (57 wt% in water; Sigma-Aldrich) in an ice bath under an argon atmosphere for 3 h. Methylammonium chloride (MACl) was synthesized by a similar procedure with the same stoichiometric amounts of methylamine and hydrochloric acid (37 wt%, Sigma-Aldrich). After the reaction, the solvent was evaporated using a rotary evaporator. MAI and MACl were washed with diethyl ether by stirring the solution for 30 min, which was repeated three times, and then finally dried at 60 °C in a vacuum oven for 24 h.[29]

Substrate and sample preparation

Glass and FTO substrates were cut into 1.2 cm × 2.5 cm and 1.2 cm × 1.5 cm rectangles respectively using a glass scribe. Each slide was hand polished using a Kimwipe until no contaminants were visible to the naked eye. The slides were then placed in a custom-made slide holder and sonicated for 10 min each in sodium dodecyl sulfate (SDS)/water, water, acetone, and then 2-propanol. All water used was purified to a resistivity of 18.2 MΩ using a Millipore Simplicity water purification system. The slides were dried using filtered, compressed air and then treated with plasma (O_2) prior to use.[30] To form the precursor solutions, MAI/CdI_2 (Sigma-Aldrich), $MACl/CdI_2$, $MAI/CdCl_2$ (Sigma-Aldrich) and $MACl/CdCl_2$ were dissolved in anhydrous *N*,*N*-dimethylformamide (DMF) at 1 : 1, 2 : 3, 1 : 1 and 2 : 1 molar ratios with the concentrations of 0.518 M, 0.518 M, 1.036 M, 1.554 M, 0.518 M, 0.518 M, 1.036 M and 0.518 M, respectively. All these precursor solutions of Cd-based materials were stirred for 3 hours at 60 °C. The $MAPbI_3$ precursor solution was synthesized using equimolar mixtures of MAI and PbI_2 in DMF, and stirred for 3 hours at ambient temperature before use. All precursor solutions were then filtered through 0.45 μm PTFE filters before use. These precursor solutions were spin coated from a homogeneous 40 wt% perovskite precursor solution at 3000 rpm for 40 s on microscope glass slides and FTO-coated glasses in nitrogen flux and then baked at 100 °C for one and a half hours to form CD-1, CD-2, CD-3, CD-4 and $MAPbI_3$ thin films.

Material characterization

Glancing incidence angle X-ray diffraction (XRD) measurements were employed on powdered materials by using a D8 ADVANCE (Bruker, Fitchburg, WI) instrument equipped with a CuKα radiation source where the incident angle was 0.4°. A Rigaku AFC12 diffractometer with a MoKα radiation source was utilized to perform single crystal XRD. UV-visible absorption spectra were recorded on a Shimadzu UV-1800 dual beam absorption spectrophotometer. Photoluminescence (PL) measurements were made on a QuantaMaster 300 fluorimeter (Photon Technology International). Time-resolved PL measurements were made using a time correlated single photon counting setup. Film samples were photoexcited using a laser head providing <200 ps pulses with a fluence of ~30 nJ cm^{-2}. A scanning electron microscopy system (SEM, Quanta 650 FEG, FEI Company, Inc., Hillsboro, OR) was used to acquire SEM figures. The beam voltage was 2 kV, to minimize electron induced damage.

Preparation of spot array photoelectrodes

Spot array electrodes (electrodes composed of spots with each spot having a different composition) were fabricated using a previously reported method[31] using a CH Instruments dispenser. The precursor solutions (0.518 M in DMF) were dispensed on the FTO substrate to create the spot array electrode. This was done by moving the piezo-dispensing tip to a programmed position over the FTO substrate, and dispensing drops ($\sim$100 pL per drop) of the precursor solutions (Fig. S1A, ESI†). The $MnCl_2$, $GeCl_2$, $EuCl_2$, $CdCl_2$, $FeCl_2$ or $CuCl_2$ precursor solution was mixed with MACl precursor solution, respectively. And then the mixed precursor solutions were dispensed in a preprogrammed pattern onto the FTO substrate. The distance between the spots on an array was about 150 μm with a spot diameter of approximately 350 μm. Each spot had a total of 25 drops. In all cases, the composition of potential hybrid perovskites included $(MA)_2MnCl_4$, $(MA)_2GeCl_4$, $(MA)_2EuCl_4$, $(MA)_2CdCl_4$, $(MA)_2FeCl_4$ and $(MA)_2CuCl_4$. The prepared arrays were annealed at 100 °C for 1.5 h in air to form these hybrid perovskites.

Screening the spot array electrodes

A schematic SECM setup has been described previously.[31] In brief, a 300 μm diameter optical fiber was connected to a 150 W xenon lamp (Oriel) and was attached to the tip holder of a CHI 900B SECM. The perovskite array was used as the working electrode and was placed in the bottom of a custom designed Teflon SECM cell with an O-ring (exposed area: 1.0 cm^2). A Pt mesh was used as the counter electrode, and a saturated $Ag/AgNO_3$ electrode was used as the reference electrode. The electrolyte consisted of 2 mM BQ and 0.1 M $TBAPF_6$ (supporting electrolyte) in DCM. Light from the xenon lamp was passed through the optical fiber, positioned perpendicular to the working electrode $\sim$200 μm above the surface, to illuminate one spot on the working electrode at a time. The optical fiber tip was scanned across the spot array electrode with a scan rate of 500 μm s^{-1}, while a potential of −0.5 V *vs.* $Ag/AgNO_3$ was applied to the working electrode through the SECM potentiostat. Scanning over the spot arrays revealed two-dimensional images indicative of the generation of photocurrent on each spot (Fig. S1B, ESI†).

Photoelectrochemical characterization

The photoactivity of methylammonium cadmium halides, CD-1, CD-2, CD-3 and CD-4, was measured in a photoelectrochemical cell by utilizing a CH Instruments model 760E electrochemical analyzer as a potentiostat. The prepared thin films were used as working electrodes (0.27 cm^2) exposed to electrolyte solution under UV-visible irradiation. In this measurement, the Cd-based hybrid material films were irradiated at the front side because the CD-1, CD-2, CD-3 and CD-4 films are too thick ($\sim$30 μm) to generate efficient charge carriers under irradiation from the back. All measurements were carried out in a fused quartz glass cell with a platinum counter electrode, $Ag/AgNO_3$ reference electrode (a silver wire immersed in 0.01 M silver nitrate in MeCN connected to the cell *via* a 0.10 M $TBAPF_6$ salt bridge), 0.1 M $TBAPF_6$ supporting electrolyte and 2 mM BQ/2 mM $BQ^{\bullet-}$ redox couples at a scan rate of 50 mV s^{-1}.[32] The photocathode (CD-1, CD-2, CD-3, CD-4 or $MAPbI_3$) and the Pt mesh counter electrode were spaced apart by $\sim$0.30 mm using a Teflon gasket, with the working electrode $<$1 mm away from the cell window. To decrease the light adsorption by the intensely colored redox species, the $BQ^{\bullet-}$/BQ solutions were kept at a low concentration. All potentials are reported *vs.* Fc/Fc^+. The UV-vis light was irradiated through the electrolyte solution using full output of the Xe lamp (XBO 150 W, Osram) with an incident light intensity of about 100 mW cm^{-2}. The supporting electrolyte was 0.1 M tetrabutylammonium hexafluorophosphate ($TBAPF_6$) in CH_2Cl_2.

Relative humidity control

For the investigation of the humidity effect, the hybrid material thin films were stored at room temperature (measured as 23 ± 1 °C) in 1000 mL controlled-humidity chambers. The relative humidity in the chambers was lessened to the desired humidity ±5% by controlling the ratio of water to glycerol.[33] The freshly activated desiccant was filled in the desiccator to maintain 0% humidity for the films. The accurate relative humidity was monitored periodically during the experiment by utilizing a calibrated hygrometer. The controlled-humidity chambers were only opened when necessary, typically once per day or less, and generally required less than 30 min to achieve the equilibrium moisture content.

Conflicts of interest

There are no conflicts to declare.

Acknowledgements

The authors acknowledge financial support from the Research Grants Council of Hong Kong (grant no. 21203518 and 9048121), City University of Hong Kong (grant no. 7004928, 6000595, 7200525, and 9680208) and Shenzhen Science Technology and Innovation Commission (grant no. R-IND12301), as well as the University of Texas at Austin (grant no. 60853646-118146).

References

1 Q. Dong, Y. Fang, Y. Shao, P. Mulligan, J. Qiu, L. Cao and J. Huang, *Science*, 2015, **347**(6225), 967–970.
2 W.-J. Yin, T. Shi and Y. Yan, *Appl. Phys. Lett.*, 2014, **104**(6), 063903.
3 C. Wehrenfennig, G. E. Eperon, M. B. Johnston, H. J. Snaith and L. M. Herz, *Adv. Mater.*, 2014, **26**(10), 1584–1589.
4 Y. Takahashi, H. Hasegawa, Y. Takahashi and T. Inabe, *J. Solid State Chem.*, 2013, **205**, 39–43.
5 K. G. Lim, H. B. Kim, J. Jeong, H. Kim, J. Y. Kim and T. W. Lee, *Adv. Mater.*, 2014, **26**(37), 6461–6466.
6 K.-G. Lim, S. Ahn, Y.-H. Kim, Y. Qi and T.-W. Lee, *Energy Environ. Sci.*, 2016, **9**(3), 932–939.

7 H. Kim, K.-G. Lim and T.-W. Lee, *Energy Environ. Sci.*, 2016, **9**(1), 12–30.
8 K. G. Lim, S. Ahn, H. Kim, M. R. Choi, D. H. Huh and T. W. Lee, *Adv. Mater. Interfaces*, 2016, **28**(34), 7515–7520.
9 N. K. Noel, S. D. Stranks, A. Abate, C. Wehrenfennig, S. Guarnera, A.-A. Haghighirad, A. Sadhanala, G. E. Eperon, S. K. Pathak and M. B. Johnston, *Energy Environ. Sci.*, 2014, **7**(9), 3061–3068.
10 W. Liao, D. Zhao, Y. Yu, C. R. Grice, C. Wang, A. J. Cimaroli, P. Schulz, W. Meng, K. Zhu and R. G. Xiong, *Adv. Mater.*, 2016, **28**(42), 9333–9340.
11 W. L. Hong, Y. C. Huang, C. Y. Chang, Z. C. Zhang, H. R. Tsai, N. Y. Chang and Y. C. Chao, *Adv. Mater.*, 2016, **28**(36), 8029–8036.
12 M. L. Lai, T. Y. Tay, A. Sadhanala, S. E. Dutton, G. Li, R. H. Friend and Z.-K. Tan, *J. Phys. Chem. Lett.*, 2016, **7**(14), 2653–2658.
13 M. Pena and J. Fierro, *Chem. Rev.*, 2001, **101**(7), 1981–2018.
14 A. Glazer, *Acta Crystallogr., Sect. B: Struct. Crystallogr. Cryst. Chem.*, 1972, **28**(11), 3384–3392.
15 D. Neagu, G. Tsekouras, D. N. Miller, H. Ménard and J. T. Irvine, *Nat. Chem.*, 2013, **5**(11), 916–923.
16 Y. Kobayashi, M. Tian, M. Eguchi and T. E. Mallouk, *J. Am. Chem. Soc.*, 2009, **131**(28), 9849–9855.
17 G. Kieslich, S. Sun and A. K. Cheetham, *Chem. Sci.*, 2014, **5**(12), 4712–4715.
18 H.-Y. Hsu, L. Ji, M. Du, J. Zhao, E. T. Yu and A. J. Bard, *J. Phys. Chem. C*, 2016, **120**(35), 19890–19895.
19 G. Chapuis, H. Arend and R. Kind, *Phys. Status Solidi A*, 1975, **31**(2), 449–454.
20 J. L. Fernández, N. Mano, A. Heller and A. J. Bard, *Angew. Chem.*, 2004, **116**(46), 6515–6517.
21 L. Gate, *Appl. Opt.*, 1974, **13**(2), 236–238.
22 Y. Zhao, X. Xu and X. You, *Sci. Rep.*, 2016, **6**, 35931.
23 Y. Li, L. Ji, R. Liu, C. Zhang, C. H. Mak, X. Zou, H.-H. Shen, S.-Y. Leu and H.-Y. Hsu, *J. Mater. Chem. A*, 2018, **6**, 12842–12875.
24 C. S. Ponseca, T. J. Savenije, M. Abdellah, K. Zheng, A. Yartsev, T. Pascher, T. Harlang, P. Chabera, T. Pullerits, A. Stepanov, J.-P. Wolf and V. Sundström, *J. Am. Chem. Soc.*, 2014, **136**(14), 5189–5192.
25 T. C. Sum and N. Mathews, *Energy Environ. Sci.*, 2014, **7**(8), 2518–2534.
26 D. Song, P. Cui, T. Wang, D. Wei, M. Li, F. Cao, X. Yue, P. Fu, Y. Li, Y. He, B. Jiang and M. Trevor, *J. Phys. Chem. C*, 2015, **119**(40), 22812–22819.
27 G. Xing, N. Mathews, S. Sun, S. S. Lim, Y. M. Lam, M. Grätzel, S. Mhaisalkar and T. C. Sum, *Science*, 2013, **342**(6156), 344–347.
28 S. D. Stranks, G. E. Eperon, G. Grancini, C. Menelaou, M. J. Alcocer, T. Leijtens, L. M. Herz, A. Petrozza and H. J. Snaith, *Science*, 2013, **342**(6156), 341–344.
29 H.-Y. Hsu, L. Ji, M. Du, J. Zhao, T. Y. Edward and A. J. Bard, *Electrochim. Acta*, 2016, **220**, 205–210.
30 J. K. Mwaura, M. R. Pinto, D. Witker, N. Ananthakrishnan, K. S. Schanze and J. R. Reynolds, *Langmuir*, 2005, **21**(22), 10119–10126.
31 J. Lee, H. Ye, S. Pan and A. J. Bard, *Anal. Chem.*, 2008, **80**(19), 7445–7450.
32 H.-Y. Hsu, L. Ji, H. S. Ahn, J. Zhao, E. T. Yu and A. J. Bard, *J. Am. Chem. Soc.*, 2015, **137**(46), 14758–14764.
33 C. F. Forney and D. G. Brandl, *HortTechnology*, 1992, **2**(1), 52–54.
34 L. Ji, H.-Y. Hsu, J. C. Lee, A. J. Bard and E. T. Yu, *Nano Lett.*, 2018, **18**, 994–1000.
35 C. Zhang, R. Liu, C. H. Mak, X. Zou, H.-H. Shen, S.-Y. Leu, L. Ji and H.-Y. Hsu, *J. Photonics Energy*, 2018, **8**, 021001.